Control of Photodynamic Motions of Azobenzene-Derivative Polymers by Laser Excitation Wavelength

Mi-Jeong Kim,* JaeDong Lee, Chaemin Chun, Dong-Yu Kim, Seiji Higuchi, Tomonobu Nakayama

The dynamic properties of photoinduced alignment and surface relief grating (SRG) formation as a function of excitation wavelength ($\lambda_{ex} = 454$, 488, 514, 532, 568, and 647 nm) are examined using five azobenzene-derivative polymers, whose absorption spectra are tuned by substituting different electron-withdrawing groups (CF_3, CN, CNCl, NO_2, $(CN)_2$). The dynamics sensitively depend on λ_{ex}. The fastest rate of photoinduced alignment is observed when λ_{ex} is between λ_{max} of the *trans* π–π^* transition and that of the *cis* n–π^* transition. A model of *trans–cis* photoisomerization has been developed based on competition between photoexcitation and relaxation, in which the n–π^* transition has a faster relaxation pathway than the π–π^* transition. Under conditions of adequate absorbance of the *trans* form at λ_{ex}, i.e., greater than $\frac{1}{2}A_{max}$, the rate of SRG formation increases at longer λ_{ex}.

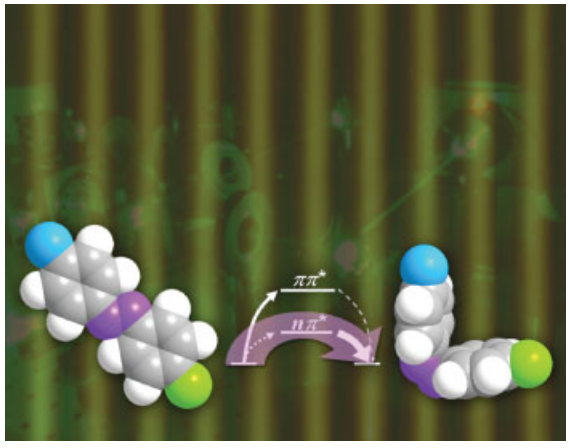

M. J. Kim, J. D. Lee
International Center for Young Scientists, National Institute for Materials Science (NIMS), 1-1 Namiki, Tsukuba, Ibaraki 305-0044, Japan
Fax: +81-29-860-4706; E-mail: kim.mijeong@nims.go.jp
J. D. Lee
School of Materials Science, Japan Advanced Institute of Science and Technology (JAIST), Ishikawa 923-1292, Japan
C. Chun, D. Y. Kim
Department of Materials Science and Engineering, Gwangju Institute of Science and Technology (GIST), 1 Oryong-dong, Buk-gu, Gwangju 500-712, Republic of Korea
S. Higuchi, T. Nakayama
Nano System Functionality Center, National Institute for Materials Science (NIMS) and the Graduate School of Pure and Applied Sciences, University of Tsukuba, 1-1 Namiki Tsukuba, Ibaraki 305-0044, Japan

Introduction

Photoisomerization is a molecular structural change between isomers caused by photoexcitation.[1] Because of the different absorption wavelength of each isomer, the functionality of materials can be switched by changing the excitation wavelength (λ_{ex}) of light: for example, photonic crystals,[2] single molecular tip,[3] magnetic materials,[4]

S. Higuchi
Technology Application R&D Department, HORIBA, Ltd., 2 Miyanohigashi, Kisshoin, Minami-ku, Kyoto 601-8510, Japan
T. Nakayama
Nanometer-scale Quantum Conductor Array Project, JST-ICORP, 4-1-8 Honcho, Kawaguchi, Saitama 332-0012, Japan

DOI: 10.1002/macp.200700159

and biomolecular activity,[5,6] etc. On the other hand, the absorption spectra can be overlapped in the visible wavelength region by substituting electron donor and acceptor groups on azobenzene.[1] A continuous *trans–cis–trans* photoisomerization cycle can then occur at the same λ_{ex}. It is a basic photonic motion that enables an azobenzene-containing polymer to respond to polarized light and an interfering laser beam. By the use of linearly polarized light, the photoisomerization cycle is minimized in a direction perpendicular to the polarization axis of the laser, so photoalignment can be achieved.[7,8] This phenomena has received much attention in the applied fields of optical data storage and plastic polarized optics.[8] In 1995, Natansohn's group and Tripathy's group independently reported an interesting photoinduced phenomenon in an azobenzene polymer film.[1,9] By irradiation with an interference laser beam, the flat surface of the film was modulated to a sinusoidal grating that had a regular periodicity. It has been suggested that photoinduced polymer mass migration occurs in the optical field, and the mobility is triggered by the photoisomerization cycle of azobenzenes.[1,9,10] Therefore, it may be expected that the dynamics of photoinduced alignment and surface relief grating (SRG) formation may have a strong correlation with the dynamics of the photoisomerization cycle.

Various structural features of azobenzenes have been investigated, such as the size of the azobenzene group,[11] the amount of azobenzene incorporated in a polymer,[12] the length of the side-chain,[13] the properties of the polymer backbone,[14] and azobenzene-derivative glasses.[15] Bulky groups bound on azobenzene exhibit a slow photoresponsive rate because of the large free volume required to change the conformation.[11] As the amount of azobenzene in a polymer is increased, the degree of photoinduced alignment increases, but intermolecular dipolar interactions among the azobenzenes and the polymeric segments start to become important at the high content.[12] This diminishes the photoinduced motions. The length of the side-chain influences the thermal mobility of the polymer and changes the phase.[13] The structural parameters related to the intermolecular interaction and thermal mobility have been intensively investigated, but there has been fewer reports on the substituents on the azobenzene that determine the key features of the photoexcited state (π–π^* or n–π^*) and the excitation wavelength of the light source. These may essentially affect the mobility in photon mode.[16] Considerable experimental and theoretical research has been performed to identify the photoisomerization pathway in gas and in solution,[17] but a general rule applicable to a series of azobenzenes has not yet been derived, especially in the polymeric film state, which is a prerequisite for many photonic applications. Recently, we investigated photodynamic properties using azobenzene polymers substituted with different electron-withdrawing groups under irradiation at fixed λ_{ex}.[18] The photoresponsive rate increases when the absorption wavelength of the *cis*-n–π^* transition approaches the λ_{ex}. In this research, the photoresponsive rates of photoinduced alignment and SRG formation as a function of λ_{ex} are examined using five azobenzene-derivative polymers whose absorption spectra are chemically tuned by substituting different electron-withdrawing groups. The observed photoresponsive rates are discussed in relation to the speed of the photoisomerization cycle and its photoexcited state.

Experimental Part

Azobenzene-Derivative Polymer Film

The chemical structure of azobenzene-derivative polymers is shown in Figure 1. The methacrylate-based azobenzene monomer and the mesogenic monomer were randomly copolymerized with a molecular ratio of 1:4, respectively. Detailed synthetic procedures were referenced in a previous report.[19] The type of electron-withdrawing group (R_1 and R_2) is given in Table 1. Amorphous polymeric films were prepared by a spin-coating process using 10 wt.-% cyclohexanone solutions at a spinning speed of 1 000 rpm onto a glass slide. The films were annealed at 70 °C in a vacuum oven for 5 h.

Characterization

The molecular weights of the polymers were measured by gel permeation chromatography (GPC, Futecs, NS2100) in a

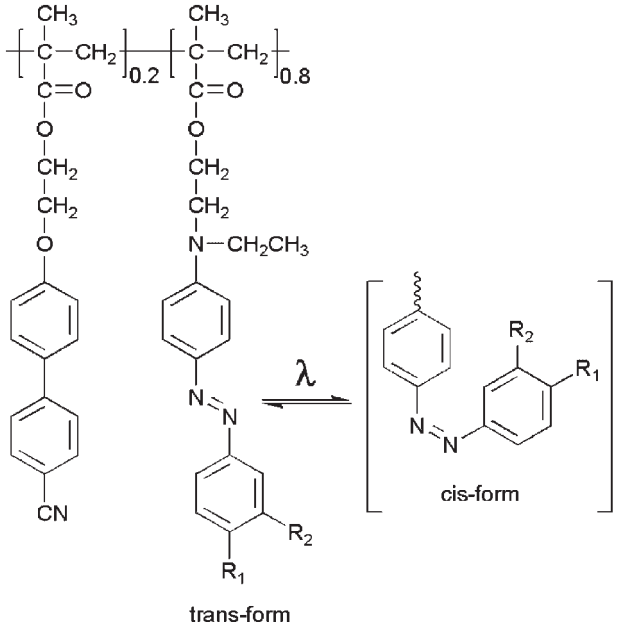

Figure 1. Chemical structure of the azobenzene-derivative polymer and its photoisomerization cycles under irradiation with visible light. The electron-withdrawing substituents, R_1 and R_2, are given in Table 1.

Macromol. Chem. Phys. **2007**, *208*, 1753–1763

Macromolecular Journals

DOI: 10.1002/macp.200700159

Table 1. Characteristic properties of the azobenzene-derivative polymers.

Sample	Substituent, X		T_g	Film thickness	λ_{max}			Dipole moment	Electron affinity
	R_1	R_2[a)]	°C	nm	nm			debye	eV
					trans	*cis* π–π^*	*cis* n–π^*		
S1	CF_3		103	450	423	410	—	6.6	1.1
S2	CN		105	440	440	372	561	6.4	1.2
S3	CN	Cl	105	480	458	378	583	7.2	1.3
S4	NO_2	CN	110	490	462	361	632	9.1	1.3
S5	CN		110	420	480	380	—	8.5	1.5

[a)]H at R_2 is omitted.

tetrahydrofuran solution calibrated against polystyrene standards. The glass transition temperature (T_g) was measured by differential scanning calorimetry (DSC2100, TA instrument) with a heating rate of 10 °C·min^{-1} under a nitrogen environment. The film thickness (d) was measured by a surface profiler (Stylus profiler, Dektak 6 M). UV-vis absorption spectra were measured using a portable UV-vis spectrometer (USB 2000, Ocean Optics) before and after laser (Coherent Verdi 2V) irradiation at 532 nm wavelength with an intensity of 50 mW·cm^{-2}. The dipole moment and electron affinity for the *trans*-azobenzene isomer were calculated with the modeling package program CAChe 6.0 workstation with PM3 parameters in the lowest energy conformations. The surface topography was examined using atomic force microscopy (AFM, SI) in the tapping mode.

Optical Setup for Photoinduced Birefringence

The optical setup for the birefringence measurement is illustrated in Figure 2(a). To provide a homogeneous beam profile over the irradiated area of the film, the laser beam was expanded through a spatial filter and collimated by a lens on a rail. The angle between the excitation laser beam and the plane of the film was 14°. Six excitation wavelengths were used: 454, 488, 514, 568, and 647 nm from an ArKr ion laser (Spectra Physics, BeamLok model 2580) and 532 nm from a diode-pumped laser (Coherent, Verdi 2V). The intensity of the collimated laser beam was 15 mW·cm^{-2}. The laser beam was polarized in the vertical direction. The polarization was confirmed by passing through a polarizer. The polarization axis (θ) was rotated to 45° using a $\lambda/2$ waveplate. The sample film was placed in the cross section of the exciting laser beam and the analyzing HeNe laser (Melles Griot, 633 nm, 0.5 mW). Two polarizers were placed before and after the film in the pathway of the HeNe laser beam with polarization axes perpendicular to each other. The transmitted intensity (I) of the HeNe laser beam was measured in situ as a function of irradiation time using a power meter (Newport, 1930C) with a time interval of 5 ms.

Optical Setup for Photoinduced SRG Formation

The SRG was optically fabricated using the Lloyd interferometer optical setup illustrated in Figure 2(b).[7,9] The laser beam was expanded using a spatial filter. This provides a convenient way to remove random fluctuations in the laser beam, and greatly improves the resolution of the holographic lithographic process. The expanded laser beam was collimated by a lens on a rail. The position of the lens was adjusted to match the focal length ($f = 10$ cm) of the lens, and the collimation state was checked using a beam collimation checker system (Sigma Koki, SPV-05-CS3). Four excitation wavelengths were used for the SRG formation: 458, 488, and 514 nm from an ArKr ion laser (Spectra Physics, BeamLok model 2580), and 532 nm from a diode-pumped laser (Coherent, Verdi 2V). The incident intensity was 15 mW·cm^{-2} at $\lambda_{ex} = 458$ nm and 50 mW·cm^{-2} at $\lambda_{ex} = 488$, 514, and 532 nm. The incident polarization was p-polarized with respect to the film plane by using a $\lambda/2$ waveplate. The relationship between the incident angle and the grating period is given by Bragg's law,

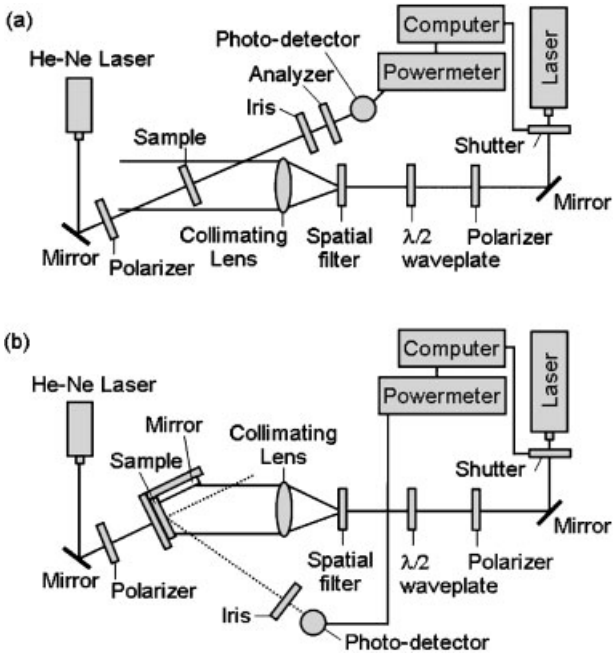

Figure 2. Optical setup for the measurement of a) photoinduced birefringence and b) SRG formation.

$\lambda_{ex} = 2d \sin\theta$, where λ_{ex} is the excitation wavelength of the laser, d is the grating period of the interference pattern, and θ is the incident angle. The incident angle (θ) of the laser beam was adjusted to fabricate a 1 μm grating period (d). The diffracted beam of a HeNe laser (Melles Griot, 633 nm, 0.5 mW) on the fabricated SRG structure was measured in situ as a function of the irradiation time. The HeNe laser was p-polarized with respect to the plane of the sample film.

Results and Discussion

Absorption Spectra of Azobenzene-Derivative Polymers

Figure 1 shows the chemical structure of the methacrylate-based azobenzene polymer used in this work. All the electron-donating substituents on azobenzene are secondary amino groups, but different electron-accepting groups are substituted at the *para* (R_1) and *meta* (R_2) positions of azobenzene. The substituent, X, designated as R_1R_2 (omitting H at the R_2 position) is indicated in Table 1. Number-averaged molecular weights ($\overline{M}_n$) are in the range of 6 000–9 000, and the T_gs are 103–110 °C. The films were prepared to have a similar thickness (d) of 456 ± 34 nm. The characteristics of the sample films are summarized in Table 1.

The *trans* isomer is the dominant component at room temperature in the dark because it is thermodynamically more stable than the *cis* isomer. For unsubstituted azobenzene, the characteristic UV-vis spectrum of the *trans* isomer has a strong π–π^* transition at 316 nm in *n*-hexane solution, and a weak n–π^* transition at 449 nm.[1] In the case of donor–acceptor substituted azobenzenes, the π–π^* band is red shifted and the n–π^* band is blue shifted, therefore, the n–π^* band is usually hidden by the intense π–π^* band.[1,20] Figure 3(a) shows UV-vis absorption spectra of the azobenzene polymer films measured at room temperature without irradiation. The maximum absorption wavelength (λ_{max}) is located at 423–480 nm, and the extent of the red shift depends on the type of substituent in the order X = $CF_3 < CN < CNCl < NO_2 < (CN)_2$. To examine the effect of the electrical characteristics on the red shift, the dipole moment and the electron affinity of the *trans*-azobenzene were calculated using the modeling program CAChe 6.0 (Table 1). The extent of red shift is proportional to the dipole moment and the electron affinity for samples S1–S4. The dipole moment of sample S5 is not the highest value among the samples, even though λ_{max} appeared at the longest wavelength. This might be because the cyanide groups (CN) are substituted at two positions on azobenzene, that is, *ortho*- and *meta*-, and have the longest hybridization length. For the other samples, the extent of the red shift is proportional to the electron-withdrawing strength of the substituent.

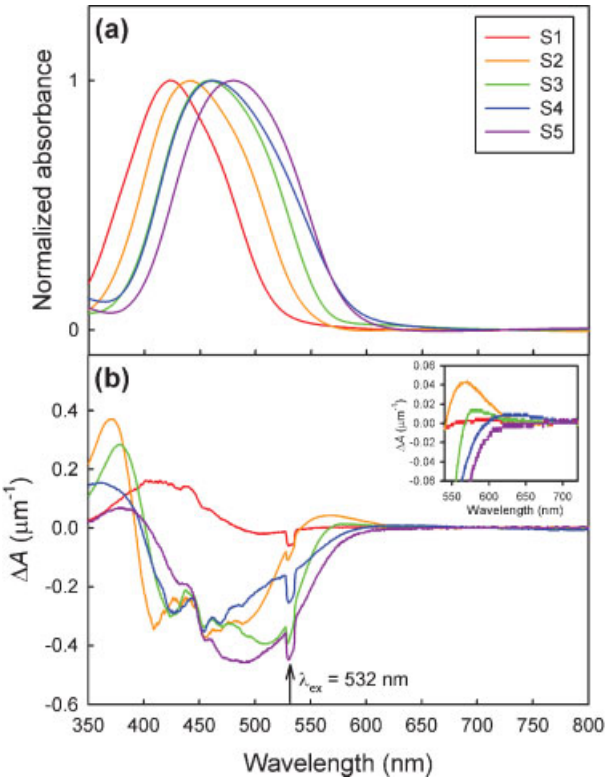

Figure 3. a) UV-vis absorption spectra of the *trans*-azobenzene polymer films measured in the dark. b) Change of absorption spectra (ΔA) by laser irradiation at a wavelength of 532 nm. $\Delta A = A_{irr} - A_d$, where A_{irr} is the absorbance during irradiation, and A_d is the absorbance before irradiation. The ΔA resulting from the *cis*-n–π^* transition is enlarged in the inset.

For azobenzene molecules in solution, the *trans* n–π^* transition is very weak because of the C_{2h} symmetry of the *trans* isomer. It has been reported that its absorption intensity is around 10% that of the *trans*-π–π^* transition.[1] When azobenzene is incorporated in a polymeric film, a higher intensity for the n–π^* transition was observed because of partial disruption of the molecular symmetry caused by the solid environment.[21] There have been a few quantitative experimental reports concerning the intensity of the n–π^* transition and λ_{max} for the donor–acceptor-type azobenzene polymer in the film state. An attempt was made to mathematically decompose the spectrum of Figure 3(a) into two bands using a combinatorial equation that contained two Gaussian functions. The resultant curves show that the hidden *trans*-n–π^* transition is located at around 60 nm higher than the *trans* π–π^* transition with about 50% of the absorption intensity of the *trans*-π–π^* transition. The absorption is much more intense than we expected. This needs to be confirmed by a proper spectroscopic method enabling the decomposition of the two overlapping bands in the future. Although the quantitative value is not clear at this moment, we should

Macromol. Chem. Phys. **2007**, *208*, 1753–1763

Macromolecular Journals
DOI: 10.1002/macp.200700159

not overlook the *trans*-n–π^* absorption for the dynamic process of the photoisomerization cycle.

The *cis*-azobenzene substituted by donor–acceptor groups has a short lifetime, and is quickly converted to the *trans* form by the laser or heat, even at room temperature.[1] The essential UV-vis spectrum of the *cis* isomer is difficult to measure directly. In this work, UV-vis spectra were taken during irradiation with the laser at $\lambda_{ex} = 532$ nm with an intensity of 50 mW·cm^{-2}. Spectroscopic information of the *cis* isomer was obtained from the *cis* component, which is generated from a steady state of the photoisomerization cycle during the irradiation. In Figure 3(b), the change of the absorbance spectrum ($\Delta A = A_{irr} - A_d$) is displayed where A_{irr} is the absorbance during irradiation, and A_d is the absorbance before irradiation. Positive bands arise from the *cis* isomer. The band below 400 nm corresponds to the *cis*-π–π^* absorption, and the peak above 540 nm corresponds to the *cis*-n–π^* absorption. In contrast to the *trans* isomer, the π–π^* band and the n–π^* band are separated by more than 180 nm. The λ_{max} values are summarized in Table 1. In the inset of Figure 3(b), the *cis*-n–π^* absorption band is enlarged. For S1 and S5, the band is not clearly shown in this experiment. For S2, S3, and S4, λ_{max} shifts to a longer wavelength as the electron-withdrawing strength of the substituent increases. This is consistent with the behavior of the *trans* isomer (Figure 3(a)).

Dynamics of Photoinduced Alignment

A ray of light is decomposed into two rays depending on the polarization when it passes through an anisotropic film. Birefringence results from different refractive indices for polarization perpendicular and parallel to the axis of anisotropy. The extent of the photoinduced alignment of azobenzene polymer films was measured in terms of birefringence using the optical setup illustrated in Figure 2(a). The detailed measurement procedures are given in the experimental section. The birefringence, Δn, was obtained using the equation, $I = I_0 \sin^2(\pi \Delta n d/\lambda p) \sin^2\theta$, where I is the intensity of the light transmitted through the crossed polarizer, I_0 is the intensity of the excitation laser beam, d is the thickness of the film, and θ is the angle between the polarization axes (45° in this work) of the exciting laser beam and the analyzing laser beam.

Figure 4 shows the birefringence curves monitored for 5 min after turning on the laser beam at $\lambda_{ex} = 532$ nm. The curves gradually increase and saturate with different speeds depending on the type of substituent. The S2 film shows the fastest growth in birefringence, and the saturated state is reached within 1 min. For a systematic comparison of the growth rate, the birefringence curves were fitted using a biexponential function, $\Delta n = A\{1 - \exp(-k_a t)\} + B\{1 - \exp(-k_b t)\}$, where t is the irradiation time, A and B are the contribution parameters, and k_a and k_b are the rate constants. This equation has been used to estimate the growing rate of birefringence since its introduction by Ho et al.[22] The inset in Figure 5 shows the result of the curve fitting. The broken line is the experimentally obtained Δn for the S2 film irradiated at $\lambda_{ex} = 514$ nm, and the solid line is the curve fitting result. The coefficient of determination (r^2) is greater than 0.92. The birefringence for the S1–S5 samples was measured for different λ_{ex}, and its fitting parameters are summarized in Table 2.

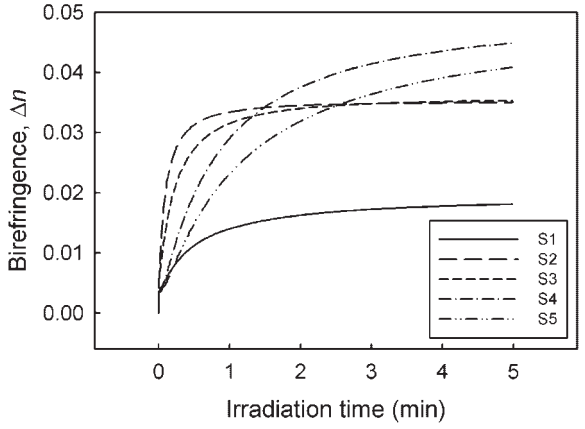

Figure 4. Photoinduced birefringence curves of films S1–S5 irradiated with an intensity of 15 mW·cm^{-2} at a wavelength of 532 nm.

The biexponential function used in the curve fitting consists of two parts; one is the fast aligning motion of the azobenzene groups, $A\{1 - \exp(-k_a t)\}$, and the other the slow aligning motion of the polymeric segments,

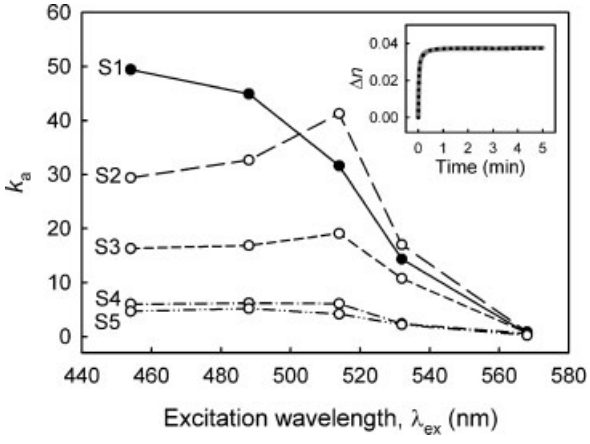

Figure 5. Plot of the fast rate constant (k_a) of the photoinduced birefringence as a function of laser λ_{ex}. The values of k_a were obtained by the curve fitting process as shown in the inset for the S2 film irradiated at $\lambda_{ex} = 514$ nm (broken line: experimental; gray solid line: fitted curve).

Table 2. Curve fitting parameters of the photoinduced birefringence.

Sample	Excitation wavelength	A ($\times 10^{-2}$)	B ($\times 10^{-2}$)	k_a	k_b
	nm			s^{-1}	s^{-1}
S1	454a	1.6	–	49.42	–
	488	1.6	0.4	44.93	5.22
	514	1.21	0.66	31.63	3.37
	532	0.64	1.15	14.35	1.03
	568[a)]	0.8	–	0.6	–
S2	454	2.31	1.06	29.41	3.13
	488	2.65	0.9	32.66	3.25
	514	2.84	0.89	41.28	4.3
	532	2.26	1.22	17.03	2.28
	568[a)]	3.9	–	0.86	–
S3	454	1.98	1.42	16.3	1.12
	488	2.08	1.51	16.87	1.33
	514	2.25	1.59	19.09	2.13
	532	1.79	1.72	10.76	1.54
	568[a)]	3.24	–	0.72	–
S4	454	1.58	1.95	6.02	0.61
	488	1.66	2.15	6.19	0.66
	514	2.9	2.49	6.1	0.83
	532	1.84	2.78	2.37	0.59
	568[a)]	4.06	–	0.58	–
S5	454	1.68	2.65	4.68	0.62
	488	1.9	2.71	5.2	0.63
	514	2.22	2.86	4.17	0.69
	532	1.19	3.12	2.21	0.52
	568[a)]	5.26	–	0.24	–

[a)]The curve was fitted with the constraint of $k_b = 0$.

$B\{1 - \exp(-k_b t)\}$. The polymeric alignment can be induced by intermolecular interaction between the aligned azobenzenes and the polymeric segment. This is a secondary effect of the photoinduced phenomenon found on the macroscopic scale.[22] To determine the photodynamic properties on the molecular level, the slow aligning speed of the polymeric segments, k_b, was excluded from consideration in this work.

In Figure 5, the rate constant of the fast molecular alignment, k_a, is plotted as a function of λ_{ex}. The value of k_a strongly depends on the type of substituent and λ_{ex}. At $\lambda_{ex} = 454$ nm, the S1 film has the highest k_a, which indicates the fastest alignment among the samples. The k_a gradually decreases in the order S1 > S2 > S3 > S4 > S5 at the given wavelength. This order implies that azobenzene substituted by strong electron-withdrawing groups tends to be more slowly aligned. To obtain rapidly aligning azobenzene polymer, a weak group such as the CF_3 of S1 needs to be substituted on the azobenzene. It should be noted that k_a is not proportional to the absorption of the *trans* form at λ_{ex}. For example, the absorption in the *trans* form is in the order S5 > S4 > S3 > S2 > S1 at $\lambda_{ex} = 532$ nm (see Figure 3(a)), but the k_a order is S2 > S1 > S3 > S4 ≈ S5 (Figure 5). The S5 film with the highest absorbance shows the lowest k_a. However, in many reports, λ_{ex} of the laser has been simply selected close to λ_{max} of the *trans* form. This might be the result of a preconception that higher absorbance of the *trans*-azobenzene polymer might have a

Macromol. Chem. Phys. **2007**, *208*, 1753–1763

Macromolecular Journals

DOI: 10.1002/macp.200700159

higher quantum yield in the photoisomerization cycles. However, from our experimental result, this is not true. Because two isomers (*trans*, *cis*) and two transition states (π–π^*, n–π^*) of each isomer participate in the photoisomerization cycles, λ_{ex} should be more carefully selected based on the spectroscopic features for the purpose of achieving fast photoresponsive speed. One clear point is that the Δn cannot be induced by irradiation outside the absorption band of the *trans* form ($\lambda_{ex} = 647$ nm). It is certain that the *trans*-to-*cis* photoisomerization cannot occur above this wavelength. When the film was excited at the tail of the *trans* absorption band ($\lambda_{ex} = 568$ nm), a small amount of Δn ($k_a = 0.24$–0.86) was slowly induced. By changing λ_{ex} from 568 to 454 nm, the k_a of the S1 film dramatically increased from 0.60 to 49.42. For the S2–S5 films, maximum values of k_a appeared. The wavelength is longer than λ_{max} of the *trans* isomer (Table 1 and Figure 3(a)). This might be caused by absorption of the *cis* isomer, which leads to *cis*-to-*trans* photoisomerization. As shown in Figure 3(b) and Table 1, λ_{max} of the *cis*-π–π^* transition and the *cis*-n–π^* transition is in the range of 380–410 nm and 561–632 nm, respectively. The *cis*-n–π^* band is located closer to the excitation wavelength of 514 nm compared with the *cis*-π–π^* transition. From the observation of maximum k_a at wavelengths longer than λ_{max} of the *trans* and shorter than the *cis*-n–π^* transition, it can be deduced that *cis*-to-*trans* photoisomerization occurs predominantly by the *cis*-n–π^* transition state.

Simulation of the *trans*-to-*cis* Photoisomerization Pathway

Besides the *cis* transition states, it is difficult to deduce a photodynamic effect related to the *trans*-π–π^* transition and the *trans*-n–π^* transition from the experimental results obtained in this work because the difference in absorption wavelengths is too small, and the *trans*-n–π^* absorbance is weak. There has been considerable effort made to determine the transition state of the photoisomerization pathway,[17] however, it is still unclear at this moment among inversion vs. rotation based on the intermediate molecular structure, or π–π^* vs. n–π^* vs. internal conversion between them, based on the electronic pathway. In this work, we have established a new model to determine the dynamic effect of transition states in *trans*-to-*cis* photoisomerization. Neither the inherent molecular symmetry nor the microscopic intramolecular interaction between the excited π–π^* and n–π^* states was addressed, and nor were extra molecular degrees of freedom such as inversion or rotation considered in this model. It may provide a general understanding on the underlying dynamic process.

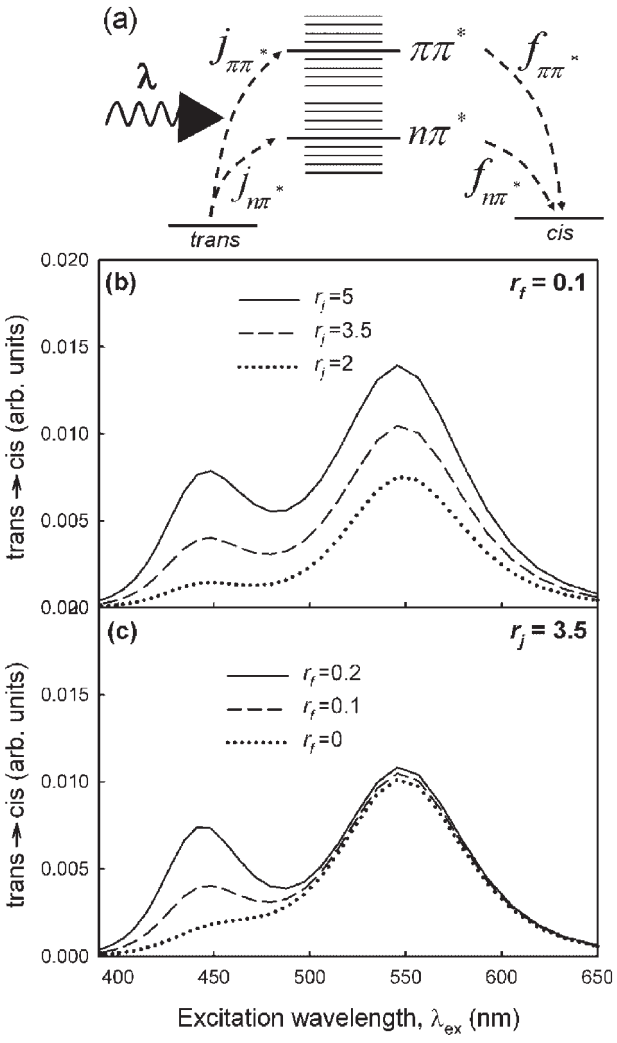

Figure 6. Model calculation of *trans*-to-*cis* photoisomerization yield with respect to excitation wavelength a) framework specifying photodynamic pathway composed of photoexcitation and relaxation. In the calculation: b) the photoexcitation from the *trans* form occurs with $r_j = 2$, 3.5, and 5, while relaxation to the *cis* form occurs with fixed $r_f = 0.1$, and c) at fixed $r_j = 3.5$, the r_f was varied as 0, 0.1, and 0.2.

Figure 6(a) describes the framework that specifies the dynamic reaction pathways of the azobenzene molecules. Choosing a pathway, the molecule initially in the *trans* state is excited to the intermediate potential surface by external laser pumping and the excited molecule then relaxes to the lower energy state, i.e., the *cis* state. We focus on the fact that both the photoexcitation and the relaxation depend on a particular pathway in a non-trivial way, which implies that the dominant pathway should be determined by the competition between photoexcitation and relaxation, depending on the pathway. For this description, a model Hamiltonian H was introduced for the molecular transition by two different π–π^* and n–π^*

pathways:

$$\begin{aligned} H &= \varepsilon_t|t\rangle\langle t| + \varepsilon_c|c\rangle\langle c| + \int d\varepsilon\varepsilon|\varepsilon\rangle\langle\varepsilon| + \int d\tilde{\varepsilon}\tilde{\varepsilon}|\tilde{\varepsilon}\rangle\langle\tilde{\varepsilon}| \\ &\quad + \iint d\varepsilon d\tilde{\varepsilon} V(\varepsilon-\varepsilon_c)[|c\rangle\langle\varepsilon| + |\varepsilon\rangle\langle c|]\left[|\tilde{\varepsilon}\rangle\langle\tilde{0}| + |\tilde{0}\rangle\langle\tilde{\varepsilon}|\right] \\ &\quad + i\int d\varepsilon j(\varepsilon)\cdot Ae^{i\omega\tau}\Theta(\tau)[|t\rangle\langle\varepsilon| - |\varepsilon\rangle\langle t|] + h.c., \end{aligned} \tag{1}$$

where ε_t, ε_c, ε, and $\tilde{\varepsilon}$ represent the energy levels of the *trans* state, the *cis* state, the intermediate continuum of the molecule, and the continuum of the energy bath, respectively. $j(\varepsilon)$ and $V(\varepsilon-\varepsilon_c)$ are the amplitudes for photoexcitation and relaxation, respectively. ω is the energy of the laser light and $\Theta(\tau)$ is the Heaviside step function.[23] The essence of the model resides in the two-pole approximation for $j(\varepsilon)$ and $V(\varepsilon-\varepsilon_c)$, which corresponds to two different pathways:

$$j(\varepsilon) = j_{n\pi*}\Delta(\varepsilon-\varepsilon_{n\pi*}) + j_{\pi\pi*}\Delta(\varepsilon-\varepsilon_{\pi\pi*}), \tag{2}$$

$$\begin{aligned} V(\varepsilon-\varepsilon_c) &= f_{n\pi*}\Delta(\varepsilon-\varepsilon_c-\varepsilon_{n\pi*}) \\ &\quad + f_{\pi\pi*}\Delta(\varepsilon-\varepsilon_c-\varepsilon_{\pi\pi*}). \end{aligned} \tag{3}$$

$\Delta(x)$ is the Lorentzian with broadening. $\varepsilon_{\pi\pi^*}$ and $\varepsilon_{n\pi^*}$ are the resonant levels that belong to the π–π^* and n–π^* bands, respectively. At $\tau=0$, the laser pumping light turns on and the wavefunction of the entire system propagates from $|\Psi(0)\rangle = |t\rangle\tilde{0}$ into $|\Psi(\tau)\rangle$:

$$\begin{aligned} |\Psi(\tau)\rangle &= \alpha(\tau)|t\rangle|\tilde{0}\rangle + \beta(\tau)|c\rangle|\tilde{0}\rangle + \int d\varepsilon\gamma(\varepsilon;\tau)|\varepsilon\rangle|\tilde{0}\rangle \\ &\quad + \int d\tilde{\varepsilon}\tilde{\alpha}(\tilde{\varepsilon};\tau)|t\rangle|\tilde{\varepsilon}\rangle + \int d\tilde{\varepsilon}\tilde{\beta}(\tilde{\varepsilon};\tau)|c\rangle|\tilde{\varepsilon}\rangle \\ &\quad + \iint d\varepsilon d\tilde{\varepsilon}\tilde{\gamma}(\varepsilon,\tilde{\varepsilon};\tau)|\varepsilon\rangle|\tilde{\varepsilon}\rangle. \end{aligned} \tag{4}$$

The time-dependent Schrödinger equation $i\frac{\partial}{\partial\tau}|\Psi(\tau)\rangle = H|\Psi(\tau)\rangle$ with $|\Psi(\tau=0)\rangle = |\tau\rangle|\tilde{0}\rangle$ gives an infinite number of coupled differential equations for the coefficients (α, β, and γ) that determine the dynamics. From the solution with $A\to 0$, the photoisomerization yield is then evaluated by:

$$I(\lambda_{ex};\tau) = \int d\tilde{\varepsilon}\left|\tilde{\beta}(\tilde{\varepsilon};\tau)\right|^2,$$

where λ_{ex} is the wavelength of the laser light used. It is found that $I(\lambda_{ex};\tau)$ quickly converged to $I(\lambda_{ex})$ as the system propagates with respect to τ.

The absorption strength $j_{\pi\pi^*}$ ($j_{n\pi^*}$) and hybridization strength $f_{\pi\pi^*}$ ($f_{n\pi^*}$) of each channel were used as the parameters to determine the photodynamics. The squares of j and f are proportional to the absorption intensity and the relaxation time, respectively. For photoexcitation, the ratio $r_j = j_{\pi\pi^*}/j_{n\pi^*}$ was used in the range of 2–5. This means the intensity of the n–π^* absorption was assumed to be in the 4–25% range of the π–π^* absorption. According to recent femtosecond time-resolved studies reported by Satzger et al.[24] using azobenzene in solution, the relaxation times of the two channels differ by about two orders of magnitude, i.e., $\propto rf2$ for $r_f = f_{\pi\pi^*}/f_{n\pi^*} \approx 0.1$. Using these experimental parameters, the dynamics started by turning on the pump beam were calculated by solving the time-dependent Schrödinger equation described above. Figure 6 shows the resulting *trans*-to-*cis* photoisomerization yield, which is dependent on the variation of the photoexcitation ratio r_j (Figure 6(b)) and the relaxation ratio r_f (Figure 6(c)). In both cases, the yield of the n–π^* excitation is higher than that of the π–π^* excitation in spite of the intense absorption in the channel of the π–π^* transition. This implies that the *trans*-to-*cis* photoisomerization is governed by the n–π^* channel because $f_{n\pi^*} \gg f_{\pi\pi^*}$ in relaxation to the *cis* form, which overwhelms $j_{n\pi^*} < j_{\pi\pi^*}$ in absorption from the *trans* form. In an actual situation, the competing peaks of the π–π^* and n–π^* transitions as in Figure 6(b) and 6(c) might be merged to a single one because of lifetime broadening and temperature broadening (not explicitly accounted for in the present model). The fastest photodynamic pathway could then be situated between $\lambda_{max}(\pi$–$\pi^*)$ and $\lambda_{max}(n$–$\pi^*)$, but shifted toward $\lambda_{max}(n$–$\pi^*)$. This is consistent with the experimental result in Figure 5.

The Dynamics of Photoinduced SRG Formation

Using the interferometric lithographic setup illustrated in Figure 2(b), the SRG was inscribed on the sample films. Figure 7 shows a characteristic surface topographic image of the SRG measured by AFM. The rate of SRG formation was examined by monitoring the intensity of the HeNe laser beam diffracted from the surface. The diffraction efficiency (DE) is defined as $DE(\%) = \frac{I}{I_0}\times 100$, where I is the diffraction intensity, and I_0 is the initial intensity of the HeNe laser. The detailed measurement procedures are given in the experimental section. Four different λ_{ex} (458, 488, 514, and 532 nm) of the interferometric laser beam were used for the SRG formation and Figure 8 is the resultant DE curve. When the film was irradiated at the shortest λ_{ex} of 458 nm, the growth rate of the DE decreased in the order S1 > S2 > S3 > S4 > S5 (Figure 8(a)) even though the order of absorption intensity of the *trans* was the opposite at this wavelength (see Figure 3(a)). This is consistent with the behavior of photoinduced alignment observed in this research (see earlier). When λ_{ex} was increased from 458 to 532 nm, the rate for the S1 film was dramatically diminished, and the slowest SRG formation was observed at $\lambda_{ex} = 532$ nm (Figure 8(a)–(d)). In order to compare the rates, the DE values at the irradiation time of

DOI: 10.1002/macp.200700159

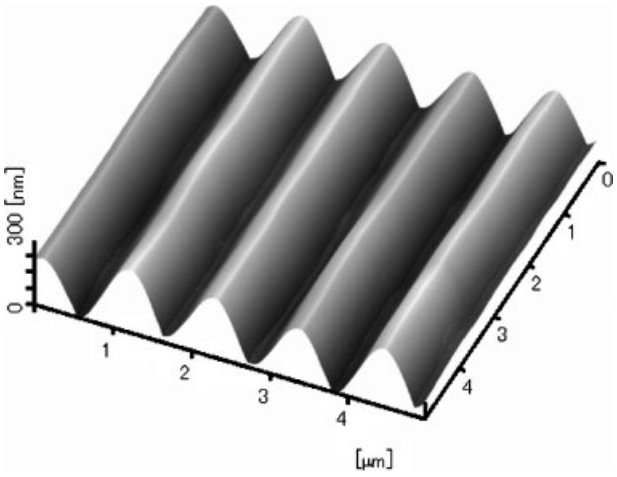

Figure 7. AFM topographic image of the SRG inscribed on the S2 film.

50 min are plotted as a function of λ_{ex} in Figure 9. Here, the DE values measured at $\lambda_{ex} = 458$ nm were excluded because the intensity of the laser beam was technically limited to below 15 mW·cm^{-2} in this experiment. Two different behaviors were observed. As longer λ_{ex} was used, S1 and S2 had smaller DE, but S3–S5 had higher DE, although the absorbance decreased. This means that excitation at the tail of the absorption band reduces the efficiency of the photoisomerization cycle (Figure 9(b)), so the rate of mass migration is also diminished. However, if the film has enough absorption at λ_{ex}, i.e., stronger than $\frac{1}{2}A_{max}$, as in Figure 9(c), longer λ_{ex} can drive faster SRG formation. Compared with the dynamic behavior of k_a in Figure 5, the increase of DE at 532 nm does not originate from photoinduced local motion such as photoisomerization cycles or alignment, but from macroscopic displacement on a micrometer-scale. Therefore, the dynamics of SRG formation could be understood as a combined process of local photoisomerization motion and macroscopic mass migration under the optical field. We are currently developing a new model for SRG formation to explain the experimentally observed dynamic behaviors and to understand the driving force generated under the interfering optical field.

Conclusion

The dynamic motions of photoalignment and mass migration to form SRG were investigated as a function of λ_{ex}, and the results are discussed in terms of the spectroscopic features of the isomers and their transition states in photoexcitation and relaxation processes. Azobenzene derivatives that have weak electron-withdrawing substituents show fast photoalignment at all laser λ_{ex}. There

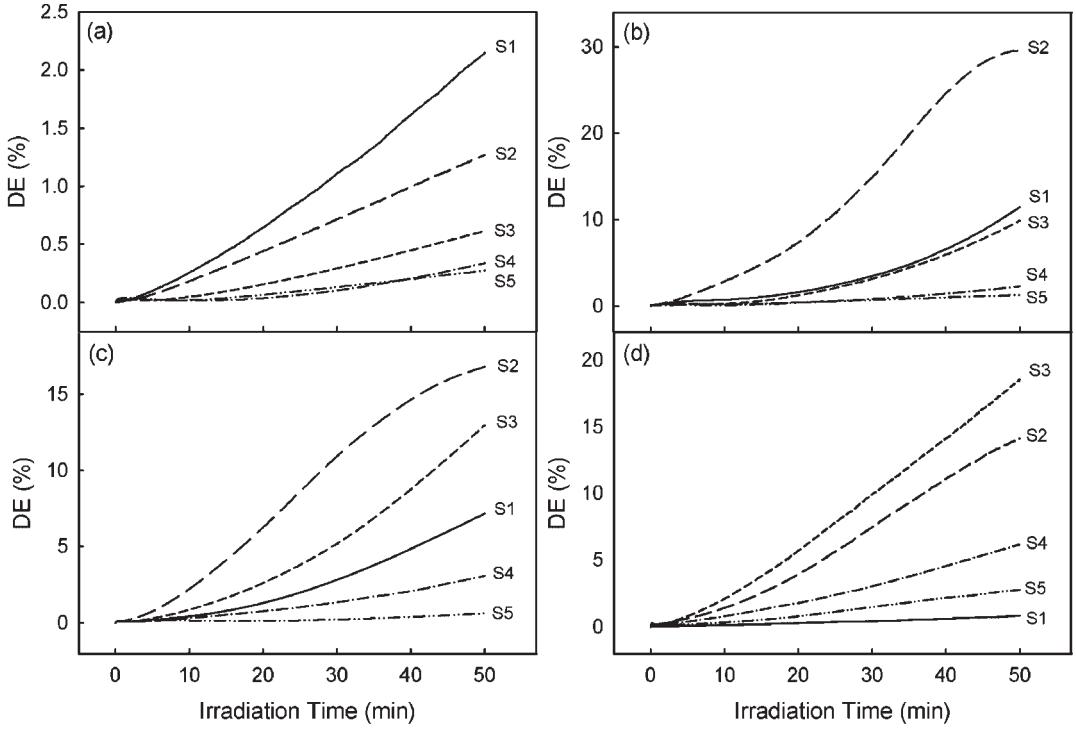

Figure 8. DE curves of SRG formation as a result of irradiation with different laser λ_{ex}: a) 458, b) 488, c) 514, and d) 532 nm. The intensity of the light was a) 15 mW·cm^{-2} and b–d) 50 mW·cm^{-2}, respectively.

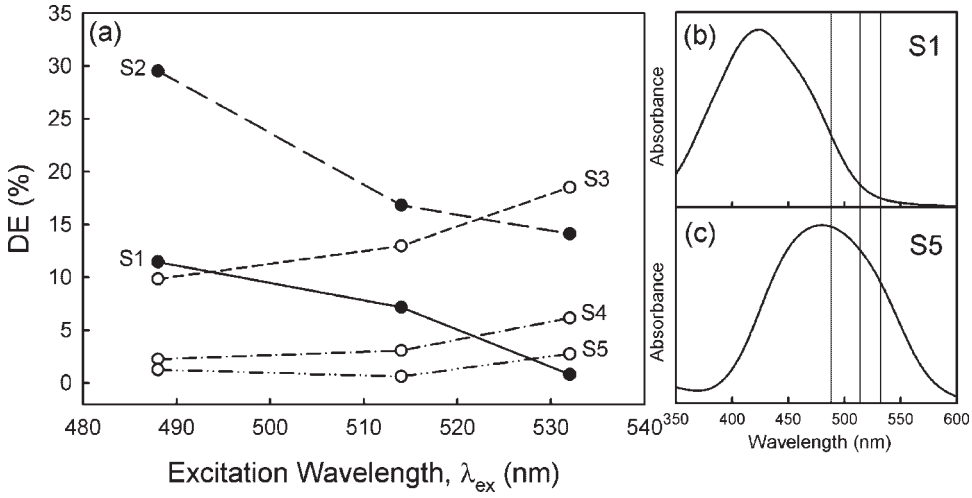

Figure 9. a) DE of SRG formation on the S1–S5 films when different λ_{ex} of the interference laser were used (intensity: 50 mW·cm^{-2}, irradiation time: 50 min, grating distance = 1 μm). b,c) UV-vis spectra of S1 and S5, the λ_{ex} (488, 514, and 532 nm) being indicated with vertical lines.

was a maximum rate of photoinduced alignment depending on the excitation wavelength, which is located between λ_{max} of the *trans* and λ_{max} of the *cis*-n–π^* transition. The rate of SRG formation increased at longer laser excitation wavelength. However, both of the rates were decreased by excitation in the tail of the absorption band. In the case of excitation over a critical absorption of the *trans* isomer, the rates did not depend on the absorption intensity. From these results, material scientists may find a guideline to select an azobenzene-derivative polymer and a laser excitation wavelength for their research purpose. The new finding of the increased rate of SRG formation at longer excitation wavelength could be a clue to understanding the mechanism of photoinduced polymeric mass migration phenomena.

Acknowledgements: The authors thank Dr. *Y. Uemura* in NIMS, Japan, for technical support. This work was financially supported by the *Special Coordination Funds for Promoting Science and Technology* from the MEXT, Japan, and *Brain Korea 21* program.

Received: March 22, 2007; Revised: May 5, 2007; Accepted: May 11, 2007; DOI: 10.1002/macp.200700159

Keywords: azobenzene-derivatives; azo-polymers; excitation wavelength; isomer/isomerism; photoisomerization; photoinduced alignment; surface relief grating

[1] [1a] G. S. Kumar, D. C. Neckers, *Chem. Rev.* **1989**, *89*, 1915; [1b] Z. Sekkat, W. Knoll, Eds., "*Photoreactive Organic Thin Films*", Academic Press, New York 2002.

[2] [2a] M. Kamenjicki, I. K. Lednev, S. A. Asher, *J. Phys. Chem. B* **2004**, *108*, 12637; [2b] S. Kubo, Z.-Z. Gu, K. Takahashi, A. Fujishima, H. Segawa, O. Sato, *Chem. Mater.* **2005**, *17*, 2298.

[3] ,D. Takamatsu, Y. Yamakoshi, K.-I. Fukui, *J. Phys. Chem. B* **2006**, *110*, 1968.

[4] [4a] Y. Einaga, O. Sato, T. Iyoda, A. Fujishima, K. Hashimoto, *J. Am. Chem. Soc.* **1999**, *121*, 3745; [4b] M. Taguchi, K. Yamada, K. Suzuki, O. Sato, Y. Einaga, *Chem. Mater.* **2005**, *17*, 4554.

[5] [5a] K. Nakayama, M. Endo, T. Majima, *Chem. Commun.* **2004**, 2386; [5b] I. Willner, S. Rubin, R. Shatzmiller, T. Zor, *J. Am. Chem. Soc.* **1993**, *19*, 8690; [5c] M. Bose, D. Groff, J. Xie, E. Brustad, P. G. Schultz, *J. Am. Chem. Soc.* **2006**, *128*, 388.

[6] A. Natansohn, P. Rochon, *Chem. Rev.* **2002**, *102*, 4139.

[7] [7a] K. Anderle, R. Birenheide, M. J. A. Werner, J. H. Wendorff, *Liq. Cryst.* **1991**, *9*, 691; [7b] T. Ubukata, T. Seki, S. Morino, K. Ichimura, *J. Phys. Chem. B* **2000**, *104*, 4148; [7c] T. Buffeteau, F. Labarthet, M. Pezolet, C. Sourisseau, *Macromolecules* **2001**, *34*, 7514; [7d] M. Ivanov, D. Ilieva, G. Minchev, Ts. Petrova, V. Dragostinova, T. Todorov, L. Nikolova, *Appl. Phys. Lett.* **2005**, *86*, 181902; [7e] J. Y. Kim, T. Fukuda, *Jpn. J. Appl. Phys.* **2006**, *45*, 456.

[8] S. Kawata, Y. Kawata, *Chem. Rev.* **2000**, *100*, 1777.

[9] [9a] P. Rochon, E. Batalla, A. Natansohn, *Appl. Phys. Lett.* **1995**, *66*, 136; [9b] D. Y. Kim, S. K. Tripathy, L. Li, J. Kumar, *Appl. Phys. Lett.* **1995**, *66*, 1166.

[10] [10a] N. K. Viswanathan, D. Y. Kim, S. Bian, J. Williams, W. Liu, L. Li, L. Samuelson, J. Kumar, S. K. Tripathy, *J. Mater. Chem.* **1999**, *9*, 1941; [10b] A. Natansohn, P. Rochon, *Chem. Rev.* **2002**, *102*, 4139; [10c] T. Ubukata, M. Hara, K. Ichimura, T. Seki, *Adv. Mater.* **2004**, *16*, 220;[10d] H. Nakano, T. Takahashi, T. Kadota, Y. Shirota, *Adv. Mater.* **2002**, *14*, 1157; [10e] F. You, M. Y. Paik, M. Häckel, L. Kador, D. Kropp, H. W. Schmidt, C. K. Ober, *Adv. Funct. Mater.* **2006**, *16*, 1577.

[11] [11a] M. S. Ho, A. Natansohn, P. Rochon, *Macromolecules* **1995**, *28*, 6124; [11b] M. S. Ho, C. Barret, J. Paterson, M. Esteghamatian, A. Natansohn, P. Rochon, *Macromolecules* **1996**, *29*, 4613.

[12] [12a] D. Brown, A. Natansohn, P. Rochon, *Macromolecules* **1995**, *28*, 6116; [12b] X. Meng, A. Natansohn, C. Barrett, P. Rochon, *Macromolecules* **1996**, *29*, 946; [12c] Y. Wu, Q. Zhang, A. Kanazawa, T. Shiono, T. Ikeda, Y. Nagase, *Macromolecules*

DOI: 10.1002/macp.200700159

1999, *32*, 3951; [12d] V. Börger, O. Kuliskovska, J. Stumpe, M. Huber, H. Menzel, *Macromol. Chem. Phys.* **2005**, *206*, 1488.
[13] [13a] S. Hvilsted, F. Andruzzi, C. Kulinna, H. W. Siesler, P. S. Ramanujam, *Macromolecules* **1995**, *28*, 2172; [13b] Y. Wu, Y. Demachi, O. Tsutsumin, A. Kanazawa, T. Shiono, T. Ikeda, *Macromolecules* **1998**, *31*, 1104; [13c] F. L. Labarthet, S. Freiberg, C. Pellerin, M. P-zolet, A. Natansohn, P. Rochon, *Macromolecules* **2000**, *33*, 6815; [13d] C. Battett, B. Choudhury, A. Natansohn, P. Rochon, *Macromolecules* **1998**, *31*, 4845;.
[14] [14a] Z. Sekkat, J. Wood, W. Knoll, W. Volken, R. D. Miller, A. Knoesen, *J. Opt. Soc. Am. B* **1997**, *14*, 829; [14b] Y. Imai, K. Naka, Y. Chujo, *Macromolecules* **1998**, *31*, 532; [14c] J. P. Chen, F. L. Labarthet, A. Natansohn, P. Rochon, *Macromolecules* **1999**, *32*, 8572; [14d] A. Izumi, M. Teraguchi, R. Nomura, T. Masuda, *Macromolecules* **2000**, *33*, 5347; [14e] Y. Wu, A. Natansohn, P. Rochon, *Macromolecules* **2001**, *34*, 7822.
[15] [15a] T. Fuhrmann, T. Tsutsui, *Chem. Mater.* **1999**, *11*, 2226; [15b] H. Nakano, T. Takahashi, T. Kadota, Y. Shirota, *Adv. Mater.* **2002**, *14*, 1157; [15c] M. J. Kim, E. M. Seo, D. Vak, D. Y. Kim, *Chem. Mater.* **2003**, *15*, 4021; [15d] E. Ishow, B. Lebon, Y. N. He, X. G. Wang, L. Bouteiller, L. Galmiche, K. Nakatani, *Chem. Mater.* **2006**, *18*, 3693; [15e] J. Gao, Y. He, H. Xu, B. Song, X. Zhang, Z. Wang, X. Wang, *Chem. Mater.* **2007**, *19*, 14.
[16] [16a] M. S. Ho, A. Natansohn, C. Barrett, P. Rochon, *Can. J. Chem.* **1995**, *73*, 1773; [16b] M. Helgert, L. Wenke, S. Hvilsted, P. S. Ramanujam, *Appl. Phys. B* **2001**, *72*, 429; [16c] C. Cojocariu, P. Rochon, *J. Mater. Chem.* **2004**, *14*, 2909.
[17] [17a] Y. Hirose, H. Yui, T. Sawada, *J. Phys. Chem. A* **2002**, *106*, 3067; [17b] T. Schultz, J. Queeneville, B. Levine, A. Toniolo, T. J. Martinex, S. Lochbrunner, M. Schmitt, J. P. Shaffer, M. Z. Zgierski, A. Stolow, *J. Am. Chem. Soc.* **2003**, *125*, 8098; [17c] T. Ishikawa, T. Noro, T. Shoda, *J. Chem. Phys.* **2001**, *115*, 7503; [17d] E. W.-G. Diau, *J. Phys. Chem. A* **2004**, *108*, 950; [17e] M. L. Tiago, S. Ismail-Beigi, S. G. Louie, *J. Chem. Phys.* **2005**, *122*, 094311; [17f] C. Ciminelli, G. Granucci, M. Persico, *Chem. Eur. J.* **2004**, *10*, 2327.
[18] M. J. Kim, C. Chun, T. Nakayama, D. Y. Kim, *Jpn. J. Appl. Phys.* **2006**, *45*, L169.
[19] [19a] D. G. Robello, *J. Polym. Sci., Part A: Polym. Chem.* **1990**, *28*, 1; [19b] G. S'heeren, A. Persoons, *Makromol. Chem.* **1993**, *194*, 1733; [19c] V. P. Shibaev, S. G. Kostromin, N. A. Plate, *Eur. Polym. J.* **1982**, *18*, 651; [19d] A. S. Angeloni, D. Caretti, C. Carlini, G. Chiellni, G. Galli, A. Altomare, R. Solaro, *Liq. Cryst.* **1989**, *4*, 513.
[20] [20a] A. A. Blevian, G. J. Blanchard, *J. Phys. Chem. B* **2004**, *108*, 4962; [20b] X. Pu, N. B. Wong, G. Zhou, J. Gu, A. Tian, *Chem. Phys. Lett.* **2005**, *408*, 101.
[21] K. Yoshii, S. Machida, K. Horie, *J. Polym. Sci., Part B: Polym. Phys.* **2000**, *38*, 3098.
[22] M. S. Ho, A. Natansohn, P. Rochon, *Macromolecules* **1995**, *28*, 6124.
[23] J. D. Lee, O. Gunnarsson, L. Hedin, *Phys. Rev. B* **1999**, *60*, 8034.
[24] H. Satzger, C. Root, M. Brown, *J. Phys. Chem. A* **2004**, *108*, 6265.